

# Seyfert 1 Composite Spectrum using SDSS Legacy Survey Data

Nihan Pol<sup>1\*</sup> and Yogesh Wadadekar,<sup>2 †</sup>

<sup>1</sup>*Department of Physics and Astronomy, West Virginia University, 135 Willey Street, Morgantown, WV 26506, United States*

<sup>2</sup>*National Centre for Radio Astrophysics, TIFR, Post Bag 3, Ganeshkhind, Pune 411007, India*

Accepted XXX. Received YYY; in original form ZZZ

## ABSTRACT

We present a rest-frame composite spectrum for Seyfert 1 galaxies using spectra obtained from the DR12 release of the Sloan Digital Sky Survey (SDSS). The spectrum is constructed by combining data from a total of 10,112 galaxies, spanning a redshift range of 0 to 0.793. We produce an electronic table of the median and geometric mean composite Seyfert 1 spectrum. We measure the spectral index of the composite spectrum, and compare it with that of the composite quasar spectrum. We also measure the flux and width of the strong emission lines present in the composite spectrum. We compare the entire spectrum with the quasar spectrum in the context of the AGN unification model. The two composite spectra match extremely well in the blue part of the spectrum, while there is an offset in flux in the red portion of the spectrum.

**Key words:** galaxies: Seyfert – galaxies: active – techniques: spectroscopic – surveys

## 1 INTRODUCTION

Seyfert galaxies are one of the most common types of Active Galactic Nuclei (AGN) in the nearby Universe. Amongst these galaxies, there are two major subclasses called Seyfert Type 1 and Seyfert Type 2 which are distinguished by their optical spectra. The spectra of Type I Seyfert galaxies show broad lines that include both allowed lines, and narrower forbidden lines. In Type I Seyfert galaxies, we are able to observe the central compact source more or less directly, therefore sampling the high velocity clouds that produce the broad emission lines from a region close to the supermassive black hole at the center of the galaxy. Seyfert nuclei are typically hosted by spiral galaxies. They are believed to be the low luminosity and low redshift counterparts of Type 1 quasars seen at higher redshifts.

The optical spectra of AGN, be they quasars, Seyfert 1s or Seyfert 2s, can be thought of as the sum of a featureless continuum and emission lines, which may be broad or narrow. Such a generic similarity between the spectra of different types of AGN is one of the drivers behind the unified model for AGN (Urry & Padovani (1995), Netzer (2015)). The basic principle of the unified model is that the underlying physical scenario for all AGNs is intrinsically similar and AGN diversity is just a geometric effect caused by different

orientation angles of the disk with respect to the observer. AGNs of the same subclass such as blazars, Seyfert 1s etc. have spectra with a number of common characteristics. Due to this, the individual spectra of specific subtypes of AGN can then be effectively combined into one single composite spectrum, which can be used to determine several median or average properties of the members of that AGN class.

For quasars, a number of efforts have been described in the literature to obtain such a composite spectrum and to use it for various scientific investigations. For instance, a composite spectrum was used to determine relative line strengths which in turn, was used to determine quasar structure (Francis et al. 1991). The composite spectrum was also used as a cross-correlation template for identification and redshift determination of quasars in SDSS data (York et al. 2000). A composite spectrum with sufficiently high signal to noise ratio can be used to find hitherto undiscovered emission lines in the spectra of quasars (Vanden Berk et al. (2001), Francis et al. (1991)). In addition to this, they can also be used for precision measurement of emission line shifts relative to laboratory wavelengths (Vanden Berk et al. (2001)), calculation of quasar colors for improved candidate selection (Richards et al. (2002)) and for calculating K-corrections used in evaluating the quasar luminosity function (Wisotzki 2000) as well as for computing the mean colours of quasars at different redshifts (White et al. 2007).

An interesting application of a composite spectrum can be seen in White et al. (2007). In order to study the radio

\* E-mail: nspol@mix.wvu.edu

† E-mail: yogesh@ncra.tifr.res.in

properties of quasars, [White et al. \(2007\)](#) make use of data from the VLA FIRST survey ([Becker et al. 1995](#)) in order to stack quasars from SDSS DR3 quasar catalog ([Schneider et al. 2005](#)). Using these data, they stack the quasars in bins based on the parameter of interest, such as redshift, or optical magnitude (see [White et al. \(2007\)](#) for more details). In particular, to study the relationship between radio luminosity and absolute magnitude, they compute the redshift dependent K-corrections using the [Vanden Berk et al. \(2001\)](#) composite quasar spectrum. If such a study for Seyfert 1 galaxies were to be undertaken, it would be necessary to have a composite spectrum for Seyfert 1 galaxies to compute the K-corrections in order to determine the radio luminosity-absolute magnitude relationship. This was one of the motivations behind this work.

For quasars, there have been several previous works aimed towards generating such a composite spectrum. [Francis et al. \(1991\)](#) generated a composite quasar spectrum using 718 quasars from the Large Bright Quasar Survey ([Foltz et al. 1989](#)). Another composite spectrum was created by [Zheng et al. \(1997\)](#) from data obtained for 284 quasars using the Hubble Space Telescope (HST) Faint Object Spectrograph. [Brotherton et al. \(2001\)](#) also prepared a composite spectrum from 657 quasars in the FIRST Bright Quasar Survey. [Vanden Berk et al. \(2001\)](#) generated a spectrum from 2204 spectra obtained from the commissioning phase of Sloan Digital Sky Survey (SDSS) ([York et al. 2000](#)). This spectrum was thereafter used as a cross-correlation template throughout the SDSS project for classification of quasars, and determining their redshifts. The most recent construction of such a composite quasar spectrum based on SDSS data was done by [Harris et al. \(2016\)](#), which contains observations of 102,150 quasars from the Baryon Oscillation Spectroscopic Survey ([Dawson et al. 2013](#)) which is a part of SDSS III ([Eisenstein et al. 2011](#)).

In comparison, there have been relatively few attempts to create such a composite optical spectrum exclusively for Seyfert galaxies, which also belong to the AGN class, but are less luminous than their quasar counterparts. An analysis was done by [Veron-Cetty et al. \(1983\)](#), who analyzed spectra of 27 Seyfert 1 nuclei in the ultraviolet band, obtained from The International Ultraviolet Explorer ([Boggess et al. 1978](#)). In this work, they binned the Seyfert 1 galaxies in three ranges of absolute luminosity, and then stacked the spectra in each of those bins to produce a composite Seyfert 1 spectrum. In addition to this, they also produced a Seyfert 1 spectrum of all the galaxies stacked together, irrespective of luminosity. They presented all these spectra in two wavelength windows, long (approximately 2000Å to 2900Å) and short (approximately 1200Å to 1900Å). [Veron-Cetty et al. \(1983\)](#), however, did not measure the spectral index for their sample of Seyfert 1 galaxies, with the study largely focused on examining emission features in the Seyfert 1 spectra. They compared their composite spectrum with a composite quasar spectrum prepared by [Wills et al. \(1980\)](#) and found that the two spectra were identical, with all the emission features observed in quasars also observed in Seyfert 1s with similar equivalent widths.

In this paper, we attempt to create a composite spectrum for Seyfert 1 galaxies which will be useful to study their global properties, and compare them with the corresponding quasar properties, particularly those listed in [Vanden Berk](#)

[et al. \(2001\)](#). Specifically, we wish to compare the continuum shape of Seyfert 1 galaxies to that of (Type 1) quasars, to test consistency with the AGN unification model. Thus, in a way, our work will be an implementation of the idea first developed by [Veron-Cetty et al. \(1983\)](#), but applied to optical wavelengths and with a much larger sample size. We also provide electronic versions of several variants of our composite Seyfert 1 spectrum.

Throughout this paper, we assume the  $\Lambda$ CDM cosmology with  $H_0 = 70 \text{ km s}^{-1} \text{ Mpc}^{-1}$ ,  $\Omega_M = 0.3$ , and  $\Omega_\Lambda = 0.7$ .

In Section 2, we describe the sample used for construction of the composite Seyfert 1 spectrum. In Section 3, we describe the methodology implemented for the creation of the spectrum, while Section 4 describes the continuum, emission and absorption features of the composite spectrum. Finally, in Section 5 we compare our results with those from [Vanden Berk et al. \(2001\)](#). Section 6 contains the conclusion.

## 2 THE SAMPLE

### 2.1 Seyfert 1 galaxies in SDSS

The candidates for the analysis presented in this paper were obtained from the most recent 13th edition of the long standing catalog of quasars and AGN published in [Véron-Cetty & Véron \(2010\)](#). This is a comprehensive catalog consisting of all known quasars and AGNs at the time of publication. The authors provide a dedicated table of AGNs, sub-classified as Seyfert 1, Seyfert 2, intermediate Seyferts, and LINERS (Table\_AGN in [Véron-Cetty & Véron \(2010\)](#)). The table lists a total of 34,231 objects, of which 17,442 are Seyfert 1, 6024 are Seyfert 2, 878 are LINERS (classified as S3 in the table), and 9,887 are unclassified. Because of the significantly larger sample, we chose to work with Seyfert 1 galaxies only.

For the work presented here, we have selected only those objects which are neither classified as Seyfert 2s nor LINERS. We have also excluded unclassified objects, even though [Véron-Cetty & Véron \(2010\)](#) suggest for them to be included as Seyfert 1 galaxies. This is due to the fact that these unclassified objects were originally classified as QSOs, but were fainter than  $M_B = -22.25$  and were consequently added to the AGN table. Thus, to prevent undue contamination by possible QSO type sources, we have excluded them from our sample.

### 2.2 Obtaining the Spectra

For each of the Seyfert 1s in the Veron-Cetty catalog, we searched for the availability of an SDSS spectrum. To do this, our sample was run through the SDSS CasJobs service in order to return the matches for these objects from the SDSS DR12 ([Alam et al. 2015](#)) database. The identification parameters for these objects, viz. plate, MJD, and fiber ID were obtained from the SpecObjAll table in CasJobs.

The requisite query returned a match with 12,429 galaxies, with a positional matching radius of 3". Of these 12,429 galaxies, 300 had a non-zero zWarning flag indicating some issue with redshift determination, and were discarded. We were then left with 12,129 galaxies.

The SDSS is a family of spectroscopic surveys comprising of Legacy ([Abazajian et al. \(2009\)](#)), BOSS ([Dawson et al.](#)

(2013)), and SEGUE (Aihara et al. (2011)) each with different strategies for targeting objects for spectroscopy, motivated by differences in their scientific goals. Of the 12,129 objects, 11,788 were drawn from the Legacy survey database, 338 from the BOSS survey database, and the remaining 3 were from the SEGUE databases. Spectra for all these objects are available from the SDSS 3 Science Archive Server (SAS). We have chosen to work only with the objects from the Legacy survey because of homogeneity in target selection. Additionally, the fiber diameter also changed from 3 arcsec in Legacy to 2 arcsec in BOSS. The SEGUE survey being designed primarily for observation of stars, the few spectra of Seyfert 1s in it are chance detections. Besides, their number is very small (3 galaxies) and are also excluded from our analysis.

These Legacy spectra have a wavelength coverage of 3800 – 9200Å, with spectral resolution in the range 1800–2200. A few of these spectra are shown in Figure 1. The spectra shown were randomly selected from different redshift bins, spanning as wide a redshift range as possible.

In addition to the above caveats, SDSS also employs a spectroscopic classification system to automatically classify a given spectrum during data processing. This system has three classes of GALAXY, QSO, and STAR, with the GALAXY class having three sub-classes, STARFORMING, STARBURST, and AGN. The input spectrum is fit with either a galaxy, QSO, or stellar template model at different redshifts. The template which provides a fit with the least chi-squared value determines the class of the object. In the case of classification as a GALAXY spectrum, if the spectrum has detectable emission lines that are consistent with being a Seyfert galaxy or a LINER, in addition to satisfying the criteria:

$$\log_{10} \left( \frac{OIII}{H\alpha} \right) > 0.7 - 1.2 \left( \log_{10} \left( \frac{NII}{H\alpha} \right) + 0.4 \right)$$

then the spectrum is sub-categorized as an AGN<sup>1</sup>.

To avoid contaminating our sample with objects whose SDSS spectra are not consistent with them being AGN, such objects were removed. Thus, we chose objects which fell under the categories of QSO or AGNs under GALAXY class, while rejecting all others with a different spectroscopic classification. Doing this leaves us with 10,162 Seyfert 1 galaxies.

A vast majority of the Seyfert 1 sample lies within redshift  $z \leq 0.8$ . Therefore, we have further truncated the sample to only include objects with redshift  $z < 0.8$ , as the number of objects beyond this range are too few in number, and their contribution to the bluest part of the rest-frame composite spectrum will be very noisy. After imposing all these conditions on sample selection, we are left with a final sample of 10,112 Seyfert 1 galaxies.

This final sample has a mean redshift  $z_{mean} = 0.263 \pm 0.149$ , with a mean absolute magnitude  $M_B = -20.543 \pm 1.138$ . In Figure 2 we plot the histogram of redshift for both the original sample of 12,129 SDSS objects and the final sample of 10,112 Seyfert 1 galaxies. Similarly, in Figure 3 we plot the histogram of the absolute magnitude of the original and final sample. These values of redshift and absolute magnitude were obtained from the same Table\_AGN that the sample was drawn from. The absolute magnitude is k-

corrected assuming an optical spectral index  $\alpha$  (defined as  $S \propto \nu^{-\alpha}$ ) equal to 0.3. In order to test whether the selection cuts to the sample changes its redshift and absolute magnitude distribution, we performed a two-sample Kolmogorov-Smirnov (KS) test with the original and final sample distributions with respect to redshift and absolute magnitude. A small p-value ( $< 0.01$ ) is required to statistically reject the null hypothesis which states that the two distributions of the final and original sample are drawn from the same underlying population. This test returned a p-value of 0.8898 for the redshift distributions, and 0.1473 for the absolute magnitude samples. This indicates that the null hypothesis cannot be rejected with high significance considering either redshift or absolute magnitude. We may then assume that our final sample is not statistically biased with respect to the original sample. We now proceed to construct a median and geometric mean composite Seyfert 1 spectrum from the final sample of 10,112 galaxies.

### 3 GENERATING THE COMPOSITE SEYFERT 1 SPECTRUM

We wish to compare the composite Seyfert 1 spectrum with the composite quasar spectrum. The best way to do so would be to compare their respective spectral indices, and check for common emission features in the spectra. To do this, it is necessary to obtain a global continuum shape for our composite spectrum, while also preserving the emission lines in the spectrum. Two different methods for combining spectra, viz. median spectrum and geometric mean spectrum are required to optimally obtain measurements of the continuum and of emission lines. The median stacking method preserves the relative fluxes of the emission features, while the geometric mean spectrum preserves the global shape of the continuum, and hence provides an accurate spectral index for the continuum. Depending on whether the emission line properties or the continuum shape are to be studied, one of these spectra will be more suitable than the other. To stack the spectra, we adopted the methodology of Vanden Berk et al. (2001). For completeness, we summarize the steps in the process here.

There are three main steps involved in the generation of a composite spectrum, viz. shifting the spectrum to rest frame, scaling of spectrum, and stacking the shifted and scaled spectrum.

At the time of Vanden Berk et al. (2001), the SDSS redshift pipeline was not sufficiently developed, and consequently, it was necessary to determine the redshift of each spectrum by examining the shift in the ubiquitous [OIII] line in the quasar spectra. However, since then, a robust redshift pipeline has become available with appropriate error flags (zWarning) indicating possible problems with measuring the redshift. Since we have already excluded galaxies with non-zero zWarning flags from our sample, we can directly use the redshift obtained from the SDSS database.

Using the SDSS redshifts, all the spectra were shifted to rest frame. Each spectrum was then re-binned into bins of width 1Å, while conserving flux. The spectra were then ordered by redshift, and the first spectrum was arbitrarily scaled. The other spectra were scaled in order of redshift to the average of the flux density in the common wavelength

<sup>1</sup> <http://www.sdss.org/dr12/spectro/catalogs/>

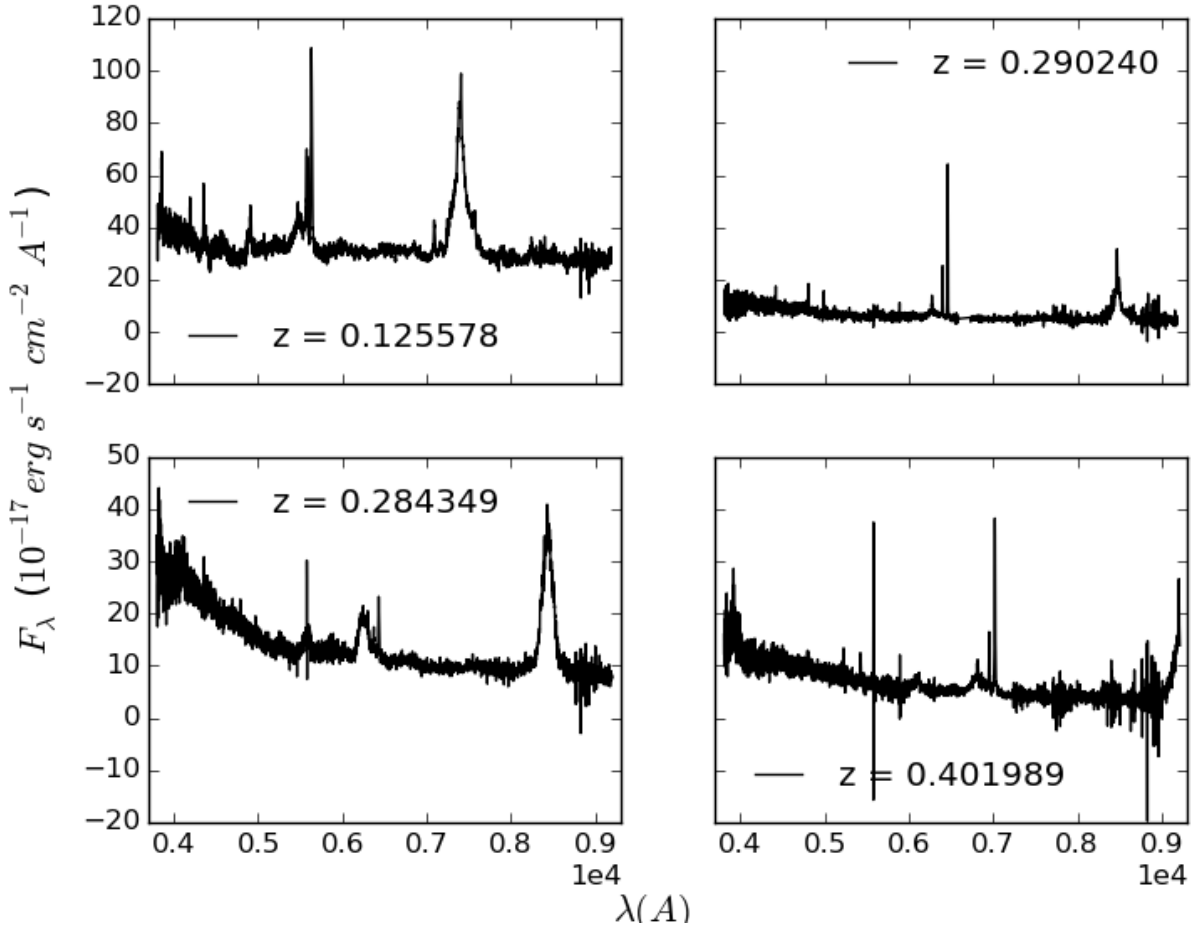


**Figure 1.** Some examples of the Seyfert 1 spectra that were used in preparing the composite spectrum. These spectra have been picked randomly from different redshift ranges.

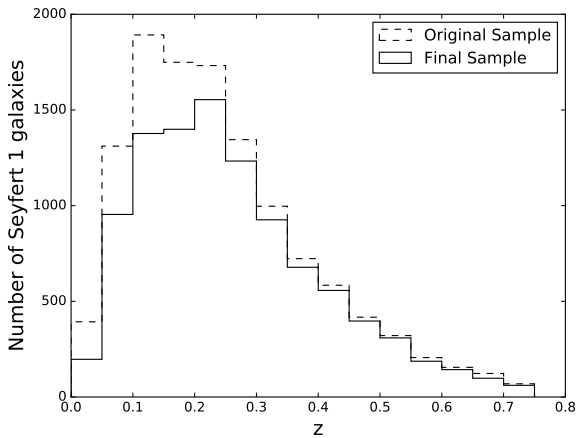


**Figure 2.** Histogram of number of galaxies per redshift bin. The number of galaxies beyond redshift of 0.8 is negligible, and hence they have been excluded from the sample.

region of the mean spectrum of all lower redshift spectra. The final spectrum was obtained by finding the median flux density in each bin of the shifted, re-binned and scaled spectra.

The median spectrum thus obtained is shown in Figure 4. The number of spectra that contribute to each bin are shown in Figure 5. An error array was also computed to determine the  $1\sigma$  deviation values for the obtained spectrum. This was done by calculating the 68% semi-interquartile range of the flux densities, divided by the square root of the number of spectra contributing to each bin. The corresponding signal-to-noise per bin obtained is shown in Figure 6.

To produce the geometric mean composite spectrum, the shifted and re-binned spectra were normalized to unit average flux density over the rest-wavelength interval 3600 – 3700Å. This interval was chosen because it contains no strong narrow emission lines. This constraint results in a total of 9812 objects contributing to the geometric mean spectrum. The number of spectra contributing to each bin in the geometric mean spectrum are shown in Figure 7. Additionally, a small number ( $\lesssim 0.4\%$ ) of pixels in the SDSS data may have negative flux values, which cannot be used

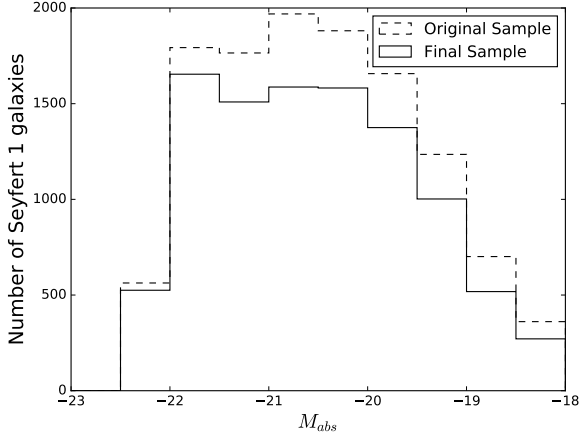


**Figure 3.** Histogram of number of galaxies per absolute magnitude bin. Véron-Cetty & Véron (2010) impose a cut-off of -22.5 absolute magnitude for the distinction between QSOs and AGNs, which is why there are no objects with absolute magnitude less than -22.5

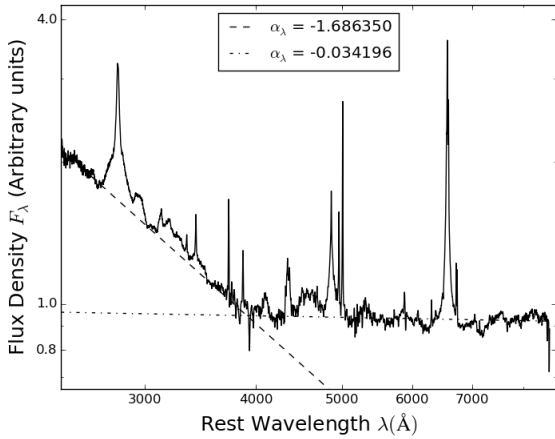


**Figure 4.** Seyfert 1 composite spectrum generated using median stacking. The figure has a log-log scale, and the power law fits to the blue and red region of the continuum are shown as dashed and dot-dashed lines respectively.

while computing a geometric mean. Such pixels were masked and not used when the geometric mean was computed. This “clipped” geometric mean spectrum is shown in Figure 8. The corresponding error, computed in the same way as for the median spectrum, is shown in Figure 9.

Both these composite spectra are available as an electronic table in the online version of this paper. The wavelength, flux, and error for a subset of the spectra are shown in Table 1.

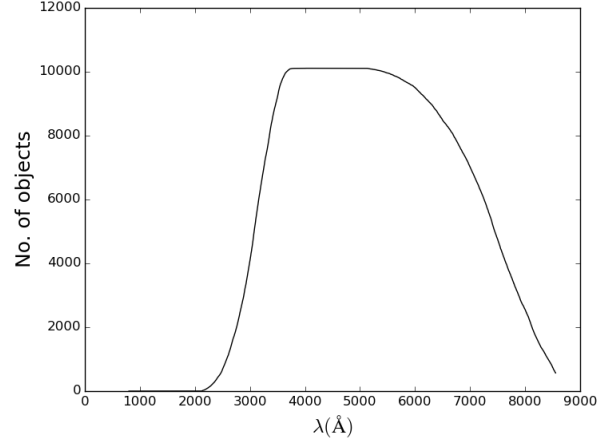


**Figure 5.** Number of spectra contributing to each 1Å bin in the median spectrum.

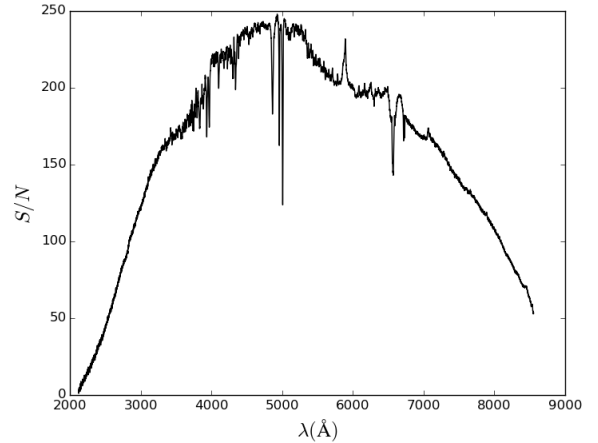


**Figure 6.** The signal-to-noise ratio for the median composite Seyfert 1 spectrum as a function of wavelength. The deep troughs correspond to emission lines in the spectrum. They are generated due to a small semi-interquartile range for the fluxes of emission lines due to approximately equal strengths of these emission lines in individual spectra.

## 4 CONTINUUM, EMISSION, AND ABSORPTION FEATURES

### 4.1 The Continuum

AGN continuum spectra are usually modeled as power-laws,

$$f_{\lambda} = \lambda^{\alpha} \quad (1)$$

where  $\alpha$  is the spectral index

The geometric mean composite spectrum is shown in Fig. 8 on a log-log plot, along with the continuum power-law fit, which appears as a straight line. Because of contamination from several strong emission lines, it is difficult to fit a curve to the entire geometric mean spectrum by conventional techniques such as a least-square fit. Therefore, we choose

Wavelength ( $\text{\AA}$ )	Flux density (arbitrary units)	Error (arbitrary units)
2122.5	1.77712735783	0.923829810185
2123.5	0.84448103612	0.84230030616
2124.5	2.57595970771	0.856977684361
2125.5	5.21397283377	1.50567701417
2126.5	1.71139567619	0.687347713267
2127.5	1.95726066225	0.64081172443
2128.5	1.59422421416	0.651461404835
2129.5	1.49231370312	0.32758731566
2130.5	2.10427057004	0.730592977066

**Table 1.** The composite median spectrum in tabular form. Only a small number of rows are shown here for guidance about its structure. The entire table is available in electronic form in the online version of this paper. The geometric mean spectrum, and the spectra binned in different redshift bins are also available online in the same format.

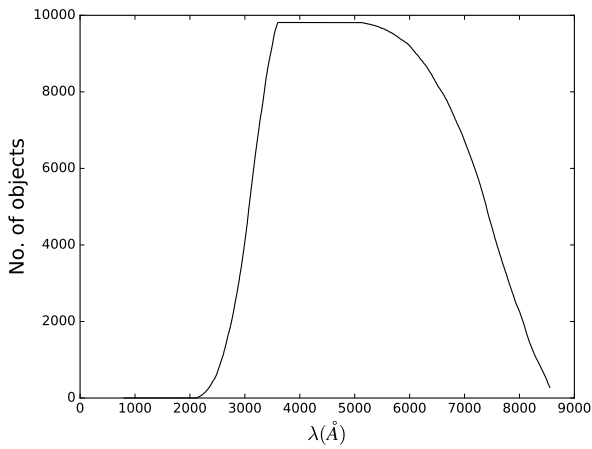


**Figure 7.** Number of spectra contributing to each  $1\text{\AA}$  bin in the geometric mean spectrum.

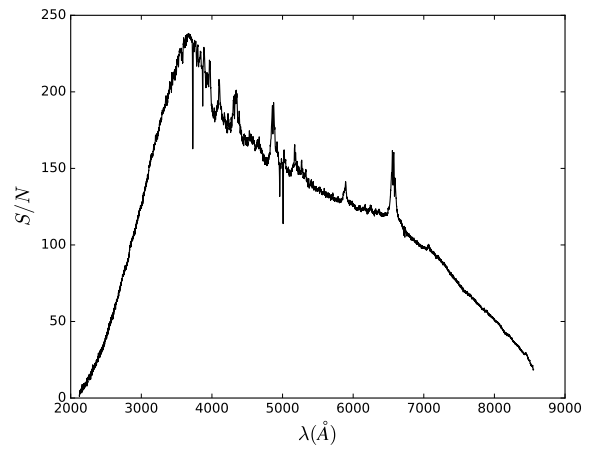


**Figure 9.** The signal-to-noise ratio for the geometric mean Seyfert 1 composite spectrum.

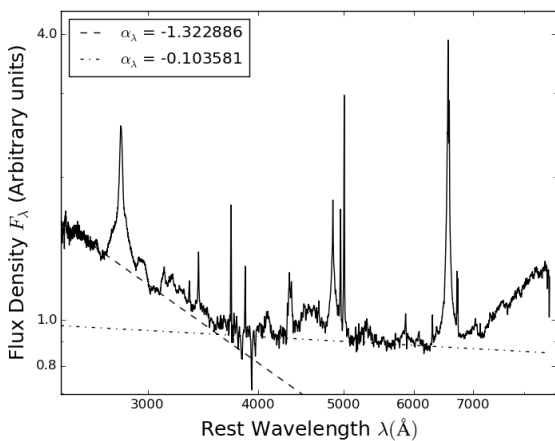


**Figure 8.** Seyfert 1 composite spectrum generated using geometric mean. The figure has log-log scale, and power law fits to the blue and red region of the continuum are shown as dashed and dot-dashed lines respectively.

two wavelength regions, situated as far away from each other as possible, which are not contaminated by strong emission lines. We then fit a power law to the data in these two regions using a non-linear least squares fit. The regions that we chose were  $2200\text{\AA} - 2220\text{\AA}$  and  $3020\text{\AA} - 3040\text{\AA}$ . Using this method, we also measure the  $1\sigma$  deviation from the median slope. The slope obtained for the geometric mean spectrum bluewards of  $H\beta$  line is  $\alpha = -1.32$ . The corresponding  $1\sigma$  value is 0.09. At wavelengths longer than that of the  $H\beta$  line, the flux rises above that predicted from the power-law fit. As a result, a different power-law fit is required for this region. The procedure for fitting a curve to this region is the same as described above, but with a region of  $4105\text{\AA} - 4125\text{\AA}$  and  $6200\text{\AA} - 6220\text{\AA}$  chosen for performing the fit. This yields a spectral index of  $\alpha = -0.1$ , with a  $1\sigma$  deviation value of 0.138.

The corresponding values obtained in [Vanden Berk et al. \(2001\)](#) for the blue and red part of the geometric mean quasar spectrum are  $\alpha = -1.56$  and  $\alpha = 0.45$  respectively. These values differ significantly from those that are obtained from the composite Seyfert 1 spectrum.

We have also fit a continuum slope to the median composite spectrum. The corresponding values are  $\alpha = -1.68$  for the blue portion of the spectrum, and  $\alpha = -0.03$  for the red portion of the spectrum. These can be compared with

the values of  $\alpha = -1.54$  and  $\alpha = -0.42$  from Vanden Berk median composite quasar spectrum respectively.

#### 4.2 Emission Features

Due to the high SNR for our median composite spectrum, we are able to clearly detect many emission lines in the median Seyfert 1 spectrum. Fig. 10 shows some of the most clearly visible lines in the median spectrum. The characteristic broad lines of *MgII* and *H $\alpha$*  are clearly visible, along with the narrower lines of [*OIII*], [*OII*], *H $\beta$*  etc. In addition, *FeII* and *FeIII* complexes can also be seen in the median spectrum. Table 2 lists the center wavelengths, measured equivalent widths, and fluxes of these lines. To compute these properties, we made use of the software package Specview. We list in Table 2 all the emission lines clearly detectable above the continuum in the median composite spectrum. We list a total of 39 emission lines, some of which are blended together in the spectrum. In the cases where we could not separate the lines, we report the flux and equivalent width of the blended line. In comparison, the median composite quasar spectrum contains 53 emission lines in the wavelength region greater than 2800Å. We did not detect any line that is not already present in the composite quasar spectrum of Vanden Berk et al. (2001).

#### 4.3 Absorption Features

We can also detect some absorption features in our median spectrum. The most prominent ones are displayed in Fig. 11. It is evident that the median composite Seyfert spectrum shows stellar absorption lines, particularly the Balmer lines and the Ca II  $\lambda 3968$  line. The presence of these lines is suggestive of stellar light contamination in the input Seyfert spectra. Just as for emission lines, we list the flux and equivalent widths of absorption lines clearly visible with respect to the continuum in Table 3.

### 5 COMPARISON WITH COMPOSITE QUASAR SPECTRUM

Fig. 12 compares our median Seyfert 1 composite spectrum with the median composite quasar spectrum from Vanden Berk et al. (2001). In producing this graph, both the spectra were normalized to unit flux in the range 3020Å – 3100Å which does not contain any strong emission features. It is obvious that the spectral index for Seyfert 1s is very similar to that of their quasar counterparts, both for the blue and red portion of the continuum. In order to see this better, Figure 13 shows the ratio of the median composite Seyfert 1 spectrum with the Vanden Berk et al. (2001) median composite quasar spectrum. In order to compute this ratio, both composite spectra were normalized to unit flux in the range 3020Å – 3100Å, after which the median composite Seyfert 1 spectrum was divided by the median composite quasar spectrum. The resulting spectrum was again normalized to have unit flux in the same wavelength region. As is evident from Figure 13, the continuum flux in the blue portion of the two composite spectra is approximately flat, while there is an offset in flux in the red portion of the spectrum. In addition to this, Figure 13 also shows the relative strength

of emission lines between the two composite spectra. For instance, the composite Seyfert 1 spectrum has, on average, stronger *MgII*, [*NeV*] and [*OIII*] lines, while the composite quasar spectrum has stronger *H $\beta$*  and *H $\alpha$*  lines. We provide this ratio spectrum in electronic form in the online version of this paper.

As can be seen, the main difference between these two spectra arises from the upturn in flux in the Seyfert 1 spectrum at approximately 4000Å. The reason for this upturn seems to be an increasing contribution of flux from the host galaxy. Our sample covers redshifts from almost 0 to 0.8. Based on the angular diameter - redshift relation for our chosen cosmology, in the lowest redshift bin (average  $z = 0.05$ ), the SDSS spectrograph fiber diameter of 3" is small enough to cover only the nuclear region of the Seyfert galaxy, while at higher redshifts, it is big enough to cover almost the whole galaxy. However, the AGN in high redshift Seyferts are, on average, more luminous than their low redshift counterparts (Gurvits et al. 1999). As a result, the light from high redshift Seyferts is dominated by the core AGN component, while that from the low redshift Seyferts shows significant contamination by host galaxy light.

To test whether this explanation is valid, we separately stacked spectra in redshift bins of width 0.1, in increasing order of redshift. A median composite spectrum was created for each of the bins in the same fashion as the complete median spectrum. The spectra produced are shown in Figure 14. If the above hypothesis is correct, we should see a decrease in the amplitude of absorption lines as we move from lower to higher redshift bins. Indeed, this is what we see when we look at the prominent absorption lines in the spectrum. This is illustrated for the CaII absorption line in Figure 15, and the measured flux and equivalent widths are given in Table 4. This trend is visible for all the other absorption lines as well.

### 6 CONCLUSION

In this paper, we have presented a composite spectrum for Seyfert type 1 galaxies. This spectrum has a sufficiently high signal to noise ratio to be useful as a template for identifying possible Seyfert 1 candidates in future spectroscopic surveys of galaxies. It may also be used to improve k-corrections in flux measurements of Seyfert galaxies at different redshifts. For this purpose, users may wish to use the binned spectra shown in Figure 14, which are made available in the online version of this paper. The composite Seyfert 1 spectrum is also remarkably similar to the composite quasar spectrum published by Vanden Berk et al. (2001). This is consistent with quasars and Seyfert 1 being the same object (Type I AGN), as predicted by the unification model of AGN.

### ACKNOWLEDGEMENTS

We thank the anonymous referee whose insightful comments improved both the content and presentation of this paper. YW acknowledges IUCAA for hosting him on his sabbatical where a part of this work was completed. Specview is a product of the Space Telescope Science Institute, which is operated by AURA for NASA.

$\lambda_{obs}$ (Å)	Amplitude (Arbitrary units)	Eq. Width (Å)	ID	$\lambda_{lab}$ or Multiplet (Å)
2797.48 ± 3.12	64.272 ± 0.784	36.10 ± 1.16	MgII	2798.75
3129.81 ± 2.69	2.273 ± 0.090	1.55 ± 0.06	OIII	3133.70
			FeII	Opt82
3344.74 ± 1.23	0.954 ± 0.055	0.74 ± 0.04	[NeV]	3346.82
3425.69 ± 0.66	3.358 ± 0.052	2.73 ± 0.04	[NeV]	3426.84
3728.62 ± 1.27	4.169 ± 0.220	4.02 ± 0.29	[OII]	3728.48
3760.55 ± 0.41	1.926 ± 0.027	2.00 ± 0.03	[FeVII]	3759.99
3783.77 ± 0.83	1.930 ± 0.045	2.03 ± 0.05	FeII	Opt15
3815.55 ± 0.97	1.767 ± 0.037	1.91 ± 0.04	FeII	Opt14
3869.12 ± 1.35	2.020 ± 0.113	2.00 ± 0.12	[NeIII]	3869.85
3891.14 ± 1.21	0.140 ± 0.017	0.14 ± 0.02	HeI	3889.74
			H8	3890.15
4072.19 ± 3.87	0.389 ± 0.082	0.40 ± 0.08	[FeV]	4072.39
4102.70 ± 0.88	0.206 ± 0.020	0.20 ± 0.02	Hδ	4102.89
4138.05 ± 2.32	0.305 ± 0.029	0.32 ± 0.09	FeII	Opt27
			FeII	Opt28
4320.82 ± 1.56	1.277 ± 0.088	1.34 ± 0.10	[FeII]	Opt21F
			FeII	Opt32
4340.93 ± 0.87	5.313 ± 0.121	5.55 ± 0.18	Hγ	4341.68
4364.21 ± 0.84	3.482 ± 0.098	3.61 ± 0.13	[OIII]	4364.44
4687.15 ± 2.28	0.681 ± 0.085	0.68 ± 0.36	HeII	4687.02
4861.79 ± 0.78	21.859 ± 0.179	22.71 ± 0.53	Hβ	4862.68
4931.32 ± 1.31	1.649 ± 0.095	1.74 ± 0.11	FeII	Opt42
4958.15 ± 0.90	7.169 ± 0.135	7.59 ± 0.23	[OIII]	4960.30
5007.77 ± 0.39	15.330 ± 0.135	16.39 ± 0.41	[OIII]	5008.24
5159.39 ± 0.92	0.489 ± 0.021	0.54 ± 0.02	[FeVII]	5160.33
5179.48 ± 0.69	0.454 ± 0.020	0.53 ± 0.02	[FeVI]	5177.48
5201.55 ± 0.78	0.589 ± 0.023	0.64 ± 0.03	[NI]	5200.53
5725.23 ± 1.49	0.590 ± 0.027	0.64 ± 0.03	[FeVII]	5722.30
5873.90 ± 1.00	1.723 ± 0.035	1.84 ± 0.04	HeI	5877.29
6083.20 ± 1.71	0.789 ± 0.034	0.86 ± 0.04	[FeVII]	6087.98
6302.72 ± 0.92	0.983 ± 0.043	1.08 ± 0.05	[OI]	6302.05
6372.78 ± 1.59	0.647 ± 0.033	0.69 ± 0.03	[OI]	6365.54
			[FeX]	6376.30
6565.39 ± 0.09	43.063 ± 0.124	47.79 ± 0.95	Hα	6564.61
6585.77 ± 0.08	22.575 ± 0.075	25.10 ± 0.38	[NII]	6585.28
6717.99 ± 0.51	3.205 ± 0.055	3.56 ± 0.07	[SII]	6718.29
6733.75 ± 0.93	2.592 ± 0.068	2.88 ± 0.09	[SII]	6732.67
7138.67 ± 1.30	0.338 ± 0.022	0.39 ± 0.02	[ArIII]	7137.80

**Table 2.** Emission lines detected in the composite Seyfert 1 spectrum. Multiplet designations for Fe are from [Vanden Berk et al. \(2001\)](#)

$\lambda_{obs}$ (Å)	Amplitude (Arbitrary units)	Eq. Width (Å)	ID	$\lambda_{lab}$ (Å)
3737.73 ± 3.18	0.507 ± 0.163	0.47 ± 0.15	H13:	3735.43
3751.09 ± 0.42	0.487 ± 0.021	0.45 ± 0.02	H12	3751.22
3771.27 ± 2.41	1.010 ± 0.069	0.93 ± 0.06	H11	3771.70
3797.96 ± 2.52	1.281 ± 0.081	1.23 ± 0.08	H10	3798.98
3835.03 ± 1.47	1.938 ± 0.059	1.91 ± 0.06	H9	3836.47
3934.67 ± 0.77	2.792 ± 0.048	2.80 ± 0.05	CaII	3934.78
3974.28 ± 0.50	0.779 ± 0.021	0.78 ± 0.02	CaII	3969.59
5895.45 ± 0.63	0.759 ± 0.019	0.79 ± 0.02	NaII	5891.58
8501.27 ± 0.63	0.821 ± 0.072	0.88 ± 0.08	CaII	8500.36
8544.80 ± 1.38	1.655 ± 0.085	1.86 ± 0.10	CaII	8544.44

**Table 3.** Strong absorption lines detected in the composite Seyfert 1 spectrum. The colon (:) in front of H13 denotes an uncertain identification due to its proximity to the [OII] emission line.



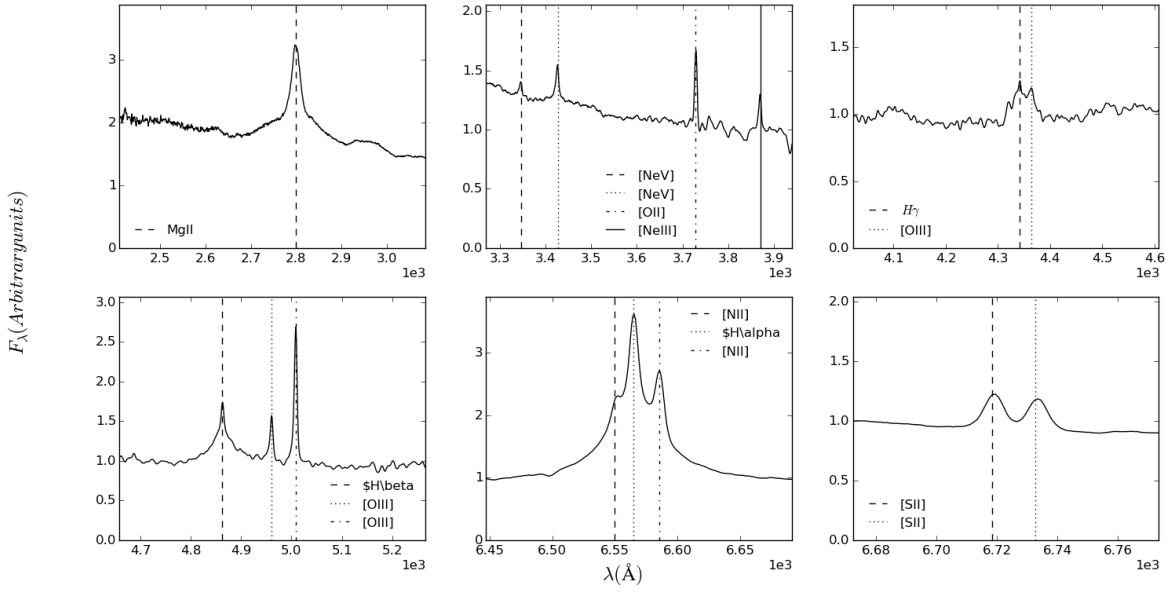


Figure 10. Strong emission line features in the composite Seyfert 1 spectrum

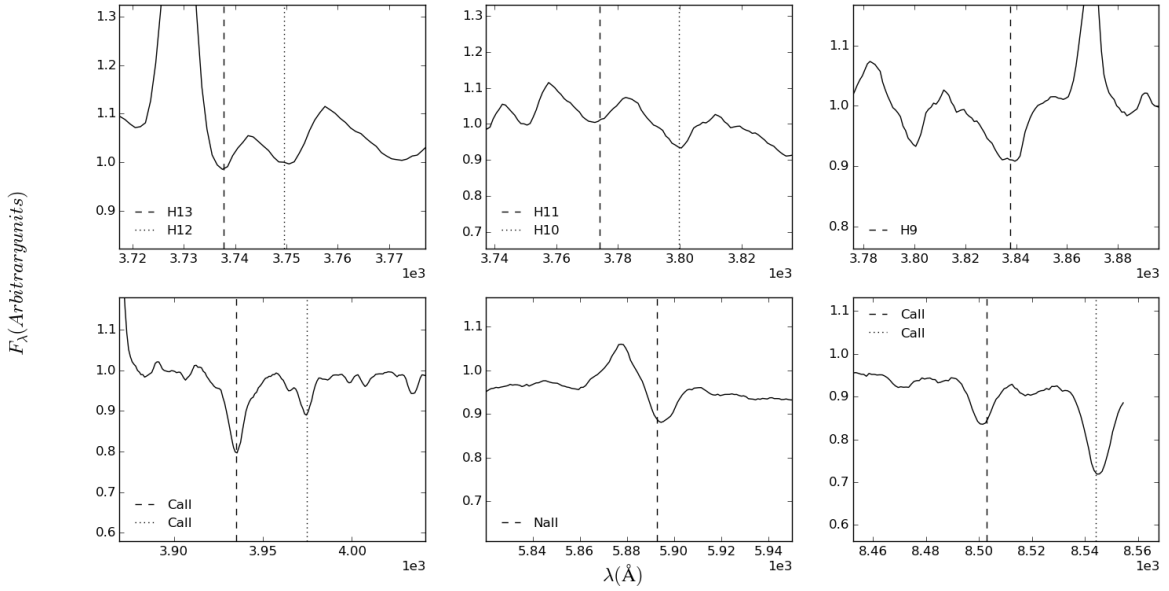
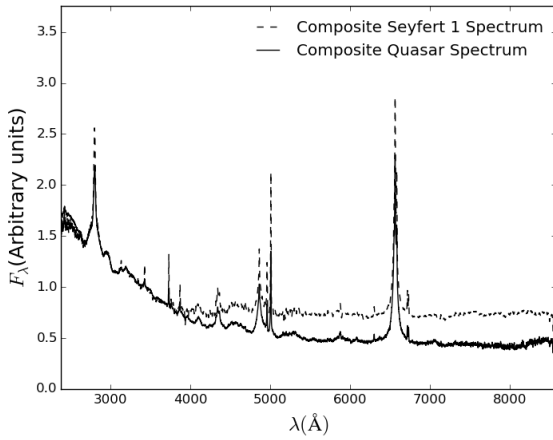


Figure 11. Absorption features in the composite Seyfert 1 spectrum. Note that the detection of H13 is uncertain due to its close proximity to the [OII] emission line.

## REFERENCES

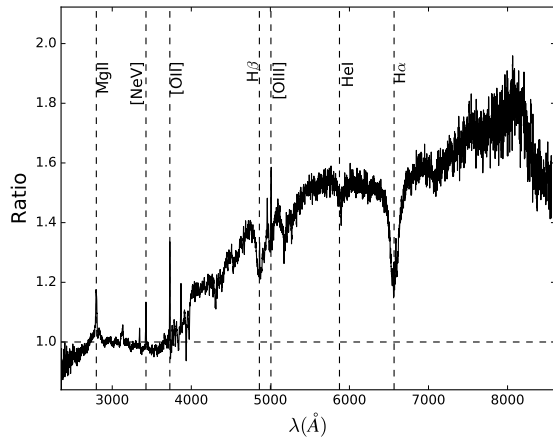
- Abazajian K. N., et al., 2009, *ApJS*, **182**, 543  
 Aihara H., et al., 2011, *ApJS*, **193**, 29  
 Alam S., et al., 2015, *The Astrophysical Journal Supplement Series*, 219, 12  
 Becker R. H., White R. L., Helfand D. J., 1995, *ApJ*, **450**, 559  
 Boggess A., et al., 1978, *Nature*, **275**, 372  
 Brotherton M. S., Tran H. D., Becker R. H., Gregg M. D., Laurent-Muehleisen S. A., White R. L., 2001, *ApJ*, **546**, 775  
 Dawson K. S., et al., 2013, *AJ*, **145**, 10  
 Eisenstein D. J., et al., 2011, *AJ*, **142**, 72  
 Foltz C. B., Chaffee F. H., Hewett P. C., Weymann R. J., Anderson S. F., MacAlpine G. M., 1989, *AJ*, **98**, 1959

Redshift bin	Amplitude (Arbitrary Units)	Eq. Width (Å)
$0.0 < z \leq 0.1$	$4.337 \pm 0.097$	$5.68 \pm 0.15$
$0.1 < z \leq 0.2$	$3.439 \pm 0.133$	$3.83 \pm 0.18$
$0.2 < z \leq 0.3$	$2.833 \pm 0.082$	$2.81 \pm 0.09$
$0.3 < z \leq 0.4$	$2.085 \pm 0.072$	$2.06 \pm 0.07$
$0.4 < z \leq 0.5$	$1.796 \pm 0.094$	$1.84 \pm 0.10$
$0.5 < z \leq 0.6$	$1.364 \pm 0.099$	$1.45 \pm 0.11$
$0.6 < z \leq 0.7$	$1.046 \pm 0.119$	$1.23 \pm 0.14$
$0.7 < z \leq 0.8$	$1.009 \pm 0.156$	$1.24 \pm 0.19$

**Table 4.** Variation in CaII absorption line strength with redshift**Figure 12.** Comparison of composite Seyfert 1 spectrum with [Vanden Berk et al. \(2001\)](#) composite quasar spectrum. Both spectra have been normalized to unit flux in the range 3020Å–3100Å. These two spectra agree remarkably well in the blue portion of the spectrum, but are offset in the red portion of the spectrum.

Francis P. J., Hewett P. C., Foltz C. B., Chaffee F. H., Weymann R. J., Morris S. L., 1991, *ApJ*, **373**, 465  
 Gurvits L. I., Kellermann K. I., Frey S., 1999, *A&A*, **342**, 378  
 Harris D. W., et al., 2016, *AJ*, **151**, 155  
 Netzer H., 2015, *ARA&A*, **53**, 365  
 Richards G. T., et al., 2002, *AJ*, **123**, 2945  
 Schneider D. P., et al., 2005, *AJ*, **130**, 367  
 Urry C. M., Padovani P., 1995, *PASP*, **107**, 803  
 Vanden Berk D. E., et al., 2001, *AJ*, **122**, 549  
 Véron-Cetty M.-P., Véron P., 2010, *A&A*, **518**, A10  
 Veron-Cetty M.-P., Tarengi M., Veron P., 1983, *A&A*, **119**, 69  
 White R. L., Helfand D. J., Becker R. H., Glikman E., de Vries W., 2007, *ApJ*, **654**, 99  
 Wills B. J., Uomoto A. K., Wills D., Netzer H., 1980, *ApJ*, **237**, 319  
 Wisotzki L., 2000, *A&A*, **353**, 861  
 York D. G., et al., 2000, *AJ*, **120**, 1579  
 Zheng W., Kriss G. A., Telfer R. C., Grimes J. P., Davidsen A. F., 1997, *ApJ*, **475**, 469

This paper has been typeset from a  $\text{\TeX}/\text{\LaTeX}$  file prepared by the author.

**Figure 13.** Ratio of median composite Seyfert 1 spectrum with median quasar composite spectrum. A few of the emission line features are labeled.

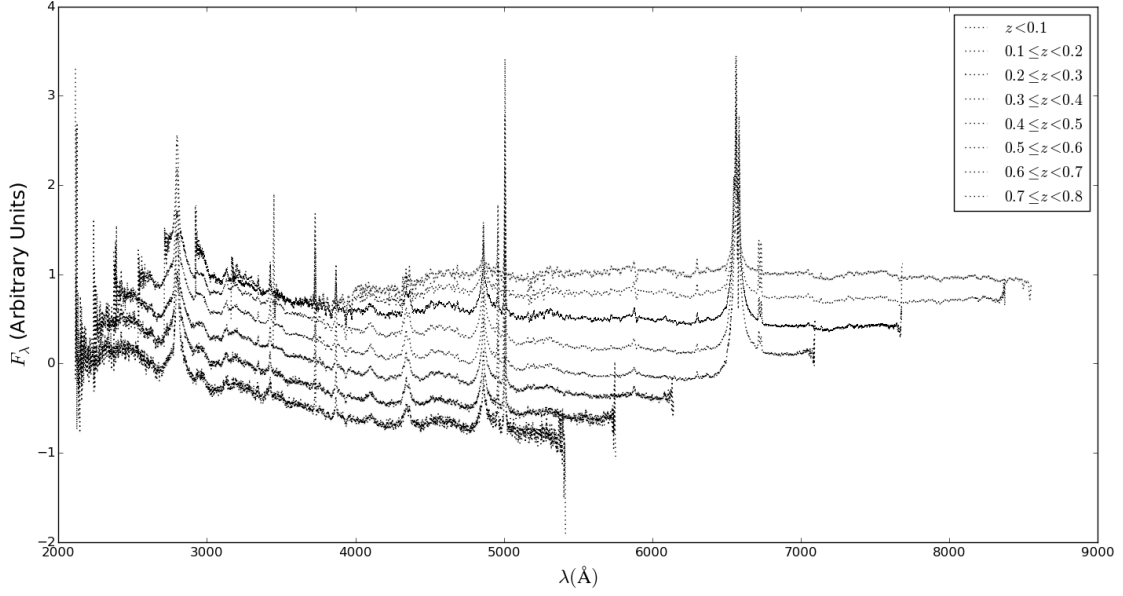


**Figure 14.** Variation in the composite Seyfert 1 spectrum with redshift. The different spectra are generated by median stacking the spectra into redshift bins of width 0.1. An offset in flux has been introduced in the stacked spectrum of successive bins for clarity. The lowest redshift bin is at the top, while higher redshift bins are progressively lower. Each spectrum is available in electronic form in the online version of this paper.

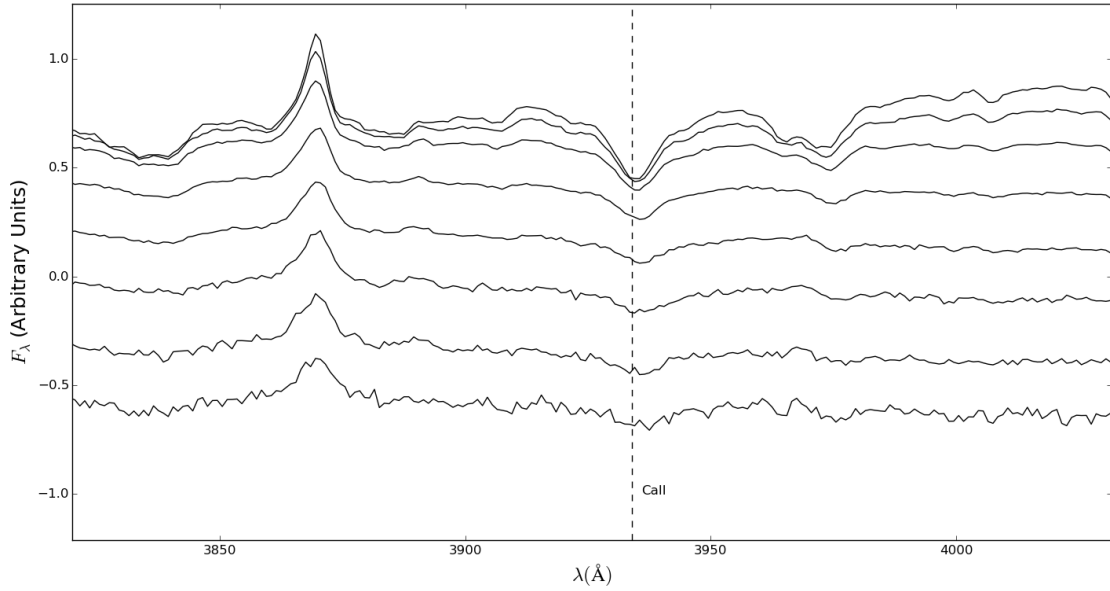


**Figure 15.** Variation in amplitude of the CaII absorption line with redshift. The spectra are ordered in increasing redshift from top to bottom. The topmost spectrum represents the bin  $0 < z < 0.1$ , the next one  $0.1 < z < 0.2$ , and so on till the last spectrum on the bottom, which represents  $0.7 < z < 0.8$ . Offsets have been introduced between each spectrum increase the visibility of each individual spectrum. The decrease in the amplitude is clearly visible with increase in redshift, with absorption lines very prominent in the lowest redshift bin, while being essentially absent in the highest redshift bin.